

Supplement of *Clim. Past*, 19, 2569–2580, 2023
<https://doi.org/10.5194/cp-19-2569-2023-supplement>
© Author(s) 2023. CC BY 4.0 License.



Supplement of

Warming drove the expansion of marine anoxia in the equatorial Atlantic during the Cenomanian leading up to Oceanic Anoxic Event 2

Mohd Al Farid Abraham et al.

Correspondence to: Mohd Al Farid Abraham (al.farid@ums.edu.my)

The copyright of individual parts of the supplement might differ from the article licence.

Supplementary Information

1. Biomarker data from ODP Leg 207 Site 1258

Table S1: Biomarker results from ODP Leg 207 Site 1258. The age model is reconstructed following the age-depth model Friedrich et al. (2008). The biomarkers shown are plotted in Figure 3, which represent the organic proxies for water column anoxia and euxinia.

Leg	Site	Hole	Core	Section	Top	Bottom	Age (Ma)	MBSF	MCD	TOC (%)	TEX86	SST (BAYSPAR)	$\frac{C_{28} \text{ 28,30-dinorhopane}}{(C_{27}-C_{35}) \text{ Hopanes (\%)}}$	$\frac{(C_{35} \text{ n-alkane} + \text{lycopane})}{C_{31} \text{ n-alkane}}$	C ₃₅ Hopanoid Thiopene (µg/g)	Isorenieratane (µg/g)
207	1258	B	45	3	44	46	93.23	399.79	420.62	13.0			3.2	2.9	0.4	0.0
207	1258	B	45	3	65	67	93.27	400.00	420.83	10.6	0.9	38.8	1.8	2.6	0.3	0.0
207	1258	B	45	4	117	118	93.53	401.93	422.76	16.2	0.9	40.6	6.1	1.1	0.4	0.0
207	1258	B	45	4	126	128	93.53	402.02	422.85	22.4	0.9	39.4	2.8	1.4	0.6	0.0
207	1258	B	45	4	130	132	93.54	402.06	422.89	26.2	0.8	35.7	2.7	1.7	0.7	0.0
207	1258	B	45	4	138	139	93.55	402.14	422.97	18.1	0.9	40.0	1.6	1.8	0.8	0.2
207	1258	B	45	4	141	143	93.55	402.17	423.00	19.7	0.9	40.0	1.8	1.3	1.2	0.2
207	1258	B	46	2	36	38	93.82	404.10	426.16	8.0	0.9	40.1	8.2	11	0.2	0.0
207	1258	B	46	2	78	80	93.85	404.52	426.58	12.7	0.9	37.0	9.5	13	0.0	0.0
207	1258	B	46	2	96	98	93.87	404.70	426.76	11.8	0.9	41.2	2.0	12	0.3	0.0
207	1258	B	46	2	100	102	93.87	404.74	426.80	6.1	0.9	36.3	2.5	1.9	0.1	0.0
207	1258	B	46	2	106	108	93.88	404.80	426.86	17.0	0.9	38.7	14	33	0.1	0.0
207	1258	B	46	2	114	116	93.88	404.88	426.94	8.5	0.9	39.4	13	32	0.1	0.0
207	1258	B	46	2	120	122	93.89	404.94	427.00	7.0	1.0	43.1	13	19	0.1	0.0
207	1258	B	46	2	126	128	93.89	405.00	427.06	10.2	0.9	39.4	12	5	0.1	0.0

207	1258	B	46	2	134	136	93.90	405.08	427.14	2.4	0.9	40.0	10	3.1	0.0	0.0
207	1258	B	46	3	78	80	93.98	406.01	428.07	8.3	0.9	36.9	3.3	1.6	0.3	0.0
207	1258	B	46	4	18	19	94.01	406.40	428.46	9.3	0.8	35.7	4.3	1.6	0.5	0.0
207	1258	B	46	4	64	65	94.05	406.86	428.92	15.0	0.9	37.5	1.8	1.5	0.4	0.0
207	1258	B	46	4	104	105	94.08	407.26	429.32	10.3	0.9	37.6	4.8	5.8	0.2	0.0
207	1258	B	47	1	52	53	94.12	407.62	429.68	10.8	0.9	39.4	2.7	2	0.0	0.0
207	1258	B	47	1	94	96	94.15	408.04	430.10	3.6	0.9	36.9	4.7	1.6	0.4	0.0
207	1258	B	47	3	73	74	94.22	409.02	431.08	8.2	0.9	36.3	5.7	5.5	0.3	0.0
207	1258	B	47	4	37	38	94.29	409.97	432.03	2.6	0.9	38.8	24	51	0.2	0.0
207	1258	B	47	4	99	100	94.44	412.03	434.09	9.3	0.9	36.9	30	51	0.3	0.0
207	1258	B	48	1	32	33	94.52	413.02	435.08	0.4	0.9	38.1	5.3	3.6	0.0	0.0
207	1258	B	48	1	108	109	94.58	413.78	435.84	9.0	0.9	36.3	3.1	1.6	0.3	0.0
207	1258	B	48	2	19	21	94.61	414.32	436.38	4.6	0.8	35.7	4.7	7.5	0.3	0.0
207	1258	B	49	1	9	11	94.80	416.79	438.85	5.8	0.8	35.7	20	39	0.2	0.0
207	1258	B	49	1	33	35	94.82	417.03	439.09	9.3	0.8	35.1	4.9	23	0.0	0.0
207	1258	B	49	1	69	71	94.85	417.39	439.45	8.9	0.8	32.6	2.9	6.6	0.0	0.0
207	1258	B	49	1	92	94	94.86	417.62	439.68	4.4	0.8	32.7	5.1	12	0.2	0.0
207	1258	B	49	1	100	102	94.87	417.70	439.76	8.0	0.8	33.3	5.7	2.2	0.0	0.0
207	1258	B	49	1	133	135	94.89	418.03	440.09	7.8	0.8	33.9	3.7	2.2	0.0	0.0
207	1258	B	49	2	6	8	94.91	418.26	440.32	4.0	0.9	37.0	9.2	40	0.2	0.0
207	1258	B	49	2	61	63	94.95	418.81	440.87	8.0	0.8	33.9	5.7	1.9	0.3	0.0
207	1258	B	49	2	81	83	94.96	419.01	441.07	7.7	0.8	33.3	2.4	2.1	0.0	0.0
207	1258	B	49	2	96	98	94.98	419.16	441.22	9.7	0.8	33.9	2.5	2.3	0.3	0.0
207	1258	B	49	3	28	30	95.01	419.65	441.71	9.9	0.8	34.5	6	15	0.0	0.0
207	1258	B	49	3	43	45	95.02	419.80	441.86	9.1	0.8	31.4	8.9	29	0.5	0.0
207	1258	B	49	4	13	15	95.05	420.09	442.15	1.7	0.8	35.1	4	3.5	0.3	0.0
207	1258	B	50	1	4	6	95.15	422.34	443.52	3.9	0.8	35.1	11	59	0.0	0.0
207	1258	B	50	1	29	31	95.16	422.59	443.77	5.8	0.8	33.2	12	19	0.0	0.0

207	1258	B	50	1	44	46	95.17	422.74	443.92	5.4	0.8	33.9	35	65	0.3	0.0
207	1258	B	50	1	64	66	95.19	422.94	444.12	9.4	0.8	33.8	7	25	0.0	0.0
207	1258	B	50	1	74	76	95.20	423.04	444.22	2.9	0.8	35.1	25	71	0.0	0.0
207	1258	B	50	2	6	8	95.26	423.80	444.98	5.3	0.8	35.7	6.2	3.5	0.1	0.0
207	1258	B	50	2	55	57	95.30	424.29	445.47	6.6	0.8	34.5	5.2	11	0.0	0.0
207	1258	B	50	3	13	15	95.35	425.10	446.28	4.5	0.9	37.0	18	20	0.0	0.0
207	1258	B	50	3	55	57	95.39	425.52	446.70	7.9	0.8	33.9	2.5	2.6	0.0	0.0
207	1258	B	51	1	14	16	95.69	426.44	450.76	2.8	0.9	38.2	19	8.1	0.0	0.0
207	1258	B	51	1	61	63	95.73	426.91	451.23	7.4	0.8	32.0	6.8	6.4	0.0	0.0
207	1258	B	51	1	87	89	95.74	427.17	451.49	10.3			1.8	2	0.2	0.0
207	1258	B	51	2	31	33	95.81	428.03	452.35	2.8	0.8	32.7	1.9	1.4	0.0	0.0
207	1258	B	51	2	117	119	95.87	428.89	453.21	7.8	0.8	33.3	1.7	0.6	0.0	0.0
207	1258	B	51	3	16	18	95.89	429.12	453.44	3.7	0.8	32.7	3.5	0.8	0.0	0.0
207	1258	B	51	3	70	72	95.93	429.66	453.98	7.6	0.8	33.3	2.5	1.3	0.0	0.0
207	1258	B	52	1	61	63	96.14	432.51	456.83	2.4	0.8	32.7	4.2	2	0.0	0.0
207	1258	B	52	2	28	30	96.20	433.29	457.61	3.3	0.8	33.9	3.4	1.5	0.0	0.0
207	1258	B	52	3	69	71	96.31	434.70	459.02	4.3	0.8	34.5	23	19	0.0	0.0
207	1258	B	52	4	12	14	96.34	435.17	459.49	7.6	0.8	33.3	2.8	2.7	0.0	0.0
207	1258	B	53	1	28	30	96.44	436.18	460.82	12.7	0.8	33.9	1.2	2.1	0.0	0.0
207	1258	B	53	2	40	42	96.54	437.50	462.14	3.5	0.8	34.5	2.4	1.7	0.0	0.0
207	1258	B	53	3	22	24	96.64	438.82	463.46	5.9	0.8	34.5	2.8	2.2	0.0	0.0
207	1258	B	54	1	47	49	96.86	441.97	466.45	1.8	0.8	34.5	3.6	7.9	0.1	0.0
207	1258	B	54	1	87	89	96.89	442.37	466.85	5.9	0.7	35.7	2.8	7.6	0.2	0.0

2. Secondary influences on GDGT distribution during Cenomanian

Table S2: Assessment on secondary influences on GDGTs distribution during Cenomanian

GDGT Indices	Cut-off value	Cenomanian average value	Interpretation
BIT Index	> 0.3	0.1	No significance influence on terrestrial influx
% GDGT-0	> 67 %	16 %	No sedimentary GDGT produce by methanogenesis.
Methane Index	> 0.5	0.2	No contribution of ammonia-oxidising archaea to GDGT pool
GDGT-2/GDGT-3	> 5	2.2	GDGTs derived from shallow planktonic community.

3. Atmospheric carbon dioxide (pCO₂) estimates from phytane δ¹³C

We use the δ¹³C values of the marine photoautotroph biomarker phytane to constrain the partial pressure of atmospheric carbon dioxide (pCO₂). Briefly, this is determined following the approach used to develop phytane-derived pCO₂ reconstructions for the Phanerozoic by Witkowski et al. (2018), adapted from previous work (i.e., Bidigare et al., 1997) and previous applications to the Cretaceous (Naafs et al., 2016; Sinninghe Damsté et al., 2008). We determine the isotope effect associated with CO₂ fixation using Equation 1 as described by Freeman and Hayes (1992):

$$\varepsilon_p = 1000 \times \left[\frac{(\delta_d + 1000)}{(\delta_p + 1000)} - 1 \right]$$

Equation 1 Isotopic CO₂ fractionation (Freeman and Hayes, 1992)

Where ε_p is overall isotopic fractionation, δ_p is the δ¹³C primary photosynthate, and δ_d is the δ¹³C of aqueous carbon dioxide (CO_{2(aq)}) in the photic zone. The δ_p is determined using Equation 2:

$$\delta_p = \delta^{13}\text{C of phytane} + \Delta\delta$$

Equation 2 δ¹³C of primary photosynthate (Freeman and Hayes, 1992)

Where δ¹³C of phytane is directly determined and Δδ is assumed to be 3.5 ‰ (σ = 1.3 ‰), based on the average of algal culture experiments that determined the offset between the δ¹³C of algal biomass and phytol (Witkowski et al., 2018).

The δ_d is normally determined using equation (3):

$$\delta_d = \delta^{13}\text{C of planktonic foraminifera} - 1 + \varepsilon_{b(a)}$$

Equation 3 δ¹³C of aqueous carbon dioxide (Freeman and Hayes, 1992)

Where δ¹³C planktonic foraminifera carbonate is measured and then adjusted for calcite-bicarbonate and bicarbonate-CO_{2(aq)} enrichment factors arising from abiotic kinetic fractionation (Romanek et al., 1992). Since the Demerara Rise sediments lack abundant, well-preserved planktonic foraminifera due to their deposition

within shoaling carbonate compensation depth (Bralower, 1988), this study applied an average value $\delta^{13}\text{C}_{\text{carb}}$ of *Whiteinella baltica* (1 ‰), as reported by Bice and Norris (2005) for the Cenomanian. This is comparable to the long-term global average of $\delta^{13}\text{C}$ for Cretaceous carbonate (1 ‰; Hayes et al., 1999). Similarly, to reconstruct CO_2 , Bice et al. (2006) applied *Hedbergella delrioensis* (0.4 ‰) and *Whiteinella baltica* (0.88 ‰), while Sinninghe Damsté et al. (2008) used a *Hedbergella delrioensis* of 2 ‰ excursions for the OAE 2. Crucially, the assumption of a constant carbonate $\delta^{13}\text{C}$ for the Cenomanian carbonate is likely incorrect, as previous records document a long-term change of about 1 ‰ across this period (Hayes et al., 1999), and that is explored in the discussion. The $\varepsilon_{\text{b(a)}}$ term reflects carbon isotopic fractionation of $(\text{CO}_2_{\text{(aq)}})$, the assumed substrate for algal photosynthesis, relative to bicarbonate; it is temperature dependant and calculated using equation (3):

$$\varepsilon_{\text{b(a)}} = 24.12 - \frac{9866}{\text{Temperature (K)}}$$

Equation 3 $\text{CO}_2(\text{aq})$ isotopic fractionation with respect to HCO_3^- – and temperature dependent (Freeman and Hayes, 1992)

The temperature is based on our reconstructed TEX_{86} -based sea surface temperature (Figure 3C) that is calibrated using BAYSPAR (Tierney and Tingley, 2014) and converted into Kelvin.

To estimate $\text{CO}_2_{\text{(aq)}}$ from ε_{p} , we use equation (4) from Bidigare et al. (1997):

$$\text{CO}_2(\text{aq}) = \frac{b}{\varepsilon_{\text{f}} - \varepsilon_{\text{p}}}$$

Equation 4 Dissolved CO_2 from photosynthetic isotopic fractionation (Bidigare et al., 1997)

This equation assumes that CO_2 enters the cell and arrives at the photosynthetic site only via diffusion (i.e. with no carbon concentrating mechanisms (Reinfelder, 2011)). Term b comprises physiological factors that influence isotopic fractionation (e.g., growth rate and cell geometry), and we estimate it to be $170 \text{ ‰ kg } \mu\text{M}^{-1}$, consistent with the previous phytane-based CO_2 reconstructions (Sinninghe Damsté et al., 2008; Witkowski et al., 2018); however, this ignores potential changes in growth rate and cell geometry. The ε_{f} value is the maximum fractionation associated with the photosynthetic fixation of carbon and is assumed to be 26.5 ‰ (Witkowski et al., 2018 and references therein).

Finally, the conversion of $\text{CO}_2_{\text{(aq)}}$ from equation (4) to $p\text{CO}_2$ is done using Henry's Law equation (5), where the solubility constant K_0 is as reported by Weiss (1974) :

$$p\text{CO}_2 = \frac{\text{CO}_2(\text{aq})}{K_0}$$

Equation 5 CO_2 conversion to $p\text{CO}_2$ using Henry's Law is respective to K_0 (Weiss, 1974)

The data used for all these calculations are presented in following Table 2.

4. Environmental Implications and $p\text{CO}_2$ reconstruction

All biomarkers record a large positive carbon isotope excursion in OAE 2 sediments. Although the limited number of OAE 2 samples we measured dictates caution, the magnitude of that shift ranges from about 2 to 7 ‰. This is larger than that inferred for the ocean-atmosphere CIE, which is thought to be 2 ‰ (Jarvis et al., 2011) but similar to the range observed at the Cape Verde Basin across OAE 2 (Sinninghe Damsté et al., 2008). This difference yields a decrease in photosynthetic carbon isotope discrimination (ϵ_p) during OAE 2. This has been attributed previously to a $p\text{CO}_2$ decline due to chemical weathering and organic carbon burial feedbacks and/or increased productivity (Sinninghe Damsté et al., 2008; Arthur et al., 1988). Our results are consistent with those interpretations. We do not focus on the MCE, which is evident in the TOC $\delta^{13}\text{C}$ data but not in the lower resolution biomarker data. Instead, we focus on the long-term Cenomanian data.

Bulk organic matter $\delta^{13}\text{C}$ data from previous work and our own (Figure 3A) are consistent with the compilation of inorganic $\delta^{13}\text{C}$ records described by Joo et al. (2020), all recording a subtle long-term increase from the middle to late Cenomanian (95.5 to 93.9 Ma). This increase also appears to be recorded in putative photoautotroph biomarkers at Demerara Rise such as phytane that has been used to reconstruct ancient $p\text{CO}_2$, including during the Cretaceous (Witkowski et al., 2018; Naafs et al., 2016), with greater discrimination during photosynthesis (or a larger difference between inorganic and organic carbon $\delta^{13}\text{C}$) indicating higher CO_2 concentrations or lower algal growth rates (Freeman and Hayes, 1992). Phytane, derived from chlorophyll, can have terrestrial sources, but that is unlikely in this setting, given the low BIT indices. Although we have not determined site-specific inorganic (carbonate) $\delta^{13}\text{C}$ values in 1258 sediments due to the low abundance of carbonate and high TOC contents, the similar trends in phytane $\delta^{13}\text{C}$ and globally widespread carbonate $\delta^{13}\text{C}$ values suggest a minimal change in carbon isotope discrimination (ϵ_p). By extension, this suggests no long-term change in $p\text{CO}_2$ despite a dramatic increase in TEX_{86} -derived SSTs.

Potentially, this is due to the very high Cenomanian $p\text{CO}_2$. At very high $p\text{CO}_2$ levels, ϵ_p values reach their maximum values dictated by the fractionation associated with the Rubisco enzyme (Pancost et al., 2013; SI Fig.1). This would also explain why phytane $\delta^{13}\text{C}$ values appear not to vary with changes in biomarker ecological or productivity proxies, which also exert a strong control on ϵ_p (Bidigare et al., 1997). Consistent with this, phytane $\delta^{13}\text{C}$ values are very low in the Cenomanian, among the lowest observed for the Phanerozoic (Witkowski et al., 2018) and perhaps reaching the limits of photosynthetic isotopic fractionation (ϵ_p) under higher $p\text{CO}_2$ conditions (Pancost et al., 2013). However, at other sites, especially those in the North American Western Interior Seaway (Joo and Sageman, 2014), TOC $\delta^{13}\text{C}$ values decrease during the Cenomanian, which Joo et al. (2020) attribute to an increase in ϵ_p driven by an increase in $p\text{CO}_2$. Such an interpretation is consistent with increasing SSTs observed at Demerara Rise and elsewhere.

There are several possible explanations for the differences between Demerara Rise and WIS long-term organic $\delta^{13}\text{C}$ records. First, there could be different local long-term trends in inorganic carbon (which had not been determined for either location). Changes in ocean circulation (e.g., upwelling) can result in local or regional trends that overprint the global changes in ocean-atmosphere $\delta^{13}\text{C}$ values. Second, at high growth rates or cell sizes, ϵ_p is more sensitive to $p\text{CO}_2$ change (Popp et al., 1998; S.I Fig.1); however, Demerara Rise is thought to be a high productivity site, which would make it more rather than less sensitive. Third, increased TOC contents and increasingly reducing conditions at Demerara Rise (Figure 3) could have been partially caused by an increase in algal growth rates. Such an increase would cause ϵ_p to decrease, potentially offsetting

an increase in ϵ_p due to higher $p\text{CO}_2$. Regardless of the mechanism, the very low phytane $\delta^{13}\text{C}$ values and insensitivity to a presumed $p\text{CO}_2$ increase are consistent with very high Cenomanian $p\text{CO}_2$ levels. Both high and rising $p\text{CO}_2$ values are likely driven by extensive volcanism during the late Cenomanian, as argued by Joo et al. (2020) and references therein.

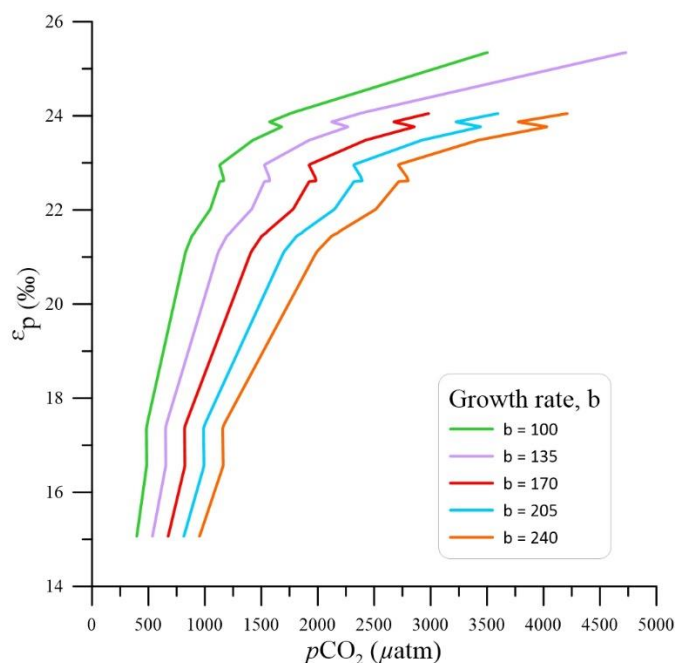


Figure S1: Relationship of sensitivity between ϵ_p (‰) value and $p\text{CO}_2$ (μatm) of Demerara Rise, with varying growth size (b). The curve represents different values of b (factors that influence the isotopic fractionation, including growth rate and cell geometry); of 100, 135, 170, 205 and 240 ‰ $\text{kg } \mu\text{M}^{-1}$, from left to right (Pancost et al., 2013).

Despite these many caveats, we can attempt to reconstruct $p\text{CO}_2$ from ϵ_p values derived from phytane $\delta^{13}\text{C}$ by assuming planktonic foraminifera $\delta^{13}\text{C}$ values of 1 ‰ (Bice and Norris, 2005) and using a biosynthetic correction factor from phytane to primary photosynthate of 3.5 ‰ (Witkowski et al., 2018). Using these assumptions, ϵ_p values range between 15 to 25.3 ‰, with the lowest fractionation during OAE 2 indicating low $p\text{CO}_2$ concentration. For the Cenomanian, this approach produces $p\text{CO}_2$ ranging from 670 to 6000 ppm (see above methods). Because the highest values of phytane-derived ϵ_p approach the nominal 26.5 ‰ maximum associated with Rubisco (Witkowski et al., 2018), these are likely underestimates of $p\text{CO}_2$. However, at such ϵ_p values, our $p\text{CO}_2$ estimates are also very sensitive to minor changes in $\delta^{13}\text{C}$ phytane. We also note that in a comparable study from Cape Verde Site 367, $\delta^{13}\text{C}$ values of free phytane are lower than those of S-bound phytane (Sinninghe Damsté et al., 2008), such that our estimates based solely on the former could overestimate the $p\text{CO}_2$.

Table S3: Carbon dioxide concentration ($p\text{CO}_2$) estimate from $\delta^{13}\text{C}$ (‰, VPDB) of phytane.

Age	MCD	SST (°C)	SST (K)	$\delta^{13}\text{C}$ (Phytane)	$\Delta\delta$	δp	δa	$\epsilon b(a)$	δd	ϵp	ϵf	b	CO2	Salinity	KO	$p\text{CO}_2$
93.54	422.89	35.7	308.9	-28.2	3.5	-24.7	1.0	-7.8	-7.8	17.3	26.5	170	18.6	35.33	0.02265	820
93.55	423.00	40.0	313.1	-27.1	3.5	-23.6	1.0	-7.4	-7.4	16.6	26.5	170	17.1	35.33	0.02081	823
93.85	426.58	37.0	310.1	-25.9	3.5	-22.4	1.0	-7.7	-7.7	15.1	26.5	170	14.9	35.33	0.02206	674
94.01	428.46	35.7	308.9	-33.3	3.5	-29.8	1.0	-7.8	-7.8	22.7	26.5	170	44.7	35.33	0.02264	1976
94.08	429.32	37.6	310.7	-34.2	3.5	-30.7	1.0	-7.6	-7.6	23.8	26.5	170	62.2	35.33	0.02180	2854
94.22	431.08	36.3	309.5	-32.1	3.5	-28.6	1.0	-7.8	-7.8	21.4	26.5	170	33.6	35.33	0.02236	1504
94.29	432.03	38.8	311.9	-32.4	3.5	-28.9	1.0	-7.5	-7.5	22.0	26.5	170	37.9	35.33	0.02129	1782
94.44	434.09	36.9	310.1	-32.1	3.5	-28.6	1.0	-7.7	-7.7	21.5	26.5	170	34.1	35.33	0.02210	1544
94.58	435.84	36.3	309.5	-31.8	3.5	-28.3	1.0	-7.8	-7.8	21.1	26.5	170	31.7	35.33	0.02236	1418
94.80	438.85	35.7	308.9	-33.3	3.5	-29.8	1.0	-7.8	-7.8	22.6	26.5	170	43.6	35.33	0.02265	1927
94.85	439.45	32.6	304.9	-36.3	3.5	-32.8	1.0	-8.2	-8.2	25.3	26.5	170	146.9	35.33	0.02467	5955
94.91	440.32	37.0	310.1	-33.1	3.5	-29.6	1.0	-7.7	-7.7	22.6	26.5	170	43.8	35.33	0.02208	1984
95.02	441.86	31.4	304.5	-34.0	3.5	-30.5	1.0	-8.3	-8.3	22.9	26.5	170	47.8	35.33	0.02488	1923
95.30	445.47	34.5	307.7	-34.7	3.5	-31.2	1.0	-7.9	-7.9	24.0	26.5	170	69.3	35.33	0.02323	2982
95.35	446.28	37.0	310.1	-32.1	3.5	-28.6	1.0	-7.7	-7.7	21.6	26.5	170	34.4	35.33	0.02206	1557
95.81	452.35	32.7	305.8	-34.8	3.5	-31.3	1.0	-8.1	-8.1	23.9	26.5	170	64.6	35.33	0.02417	2674
96.64	463.46	34.5	307.6	-34.2	3.5	-30.7	1.0	-7.9	-7.9	23.5	26.5	170	56.3	35.33	0.02324	2423